Supporting Information

A Docked State Conformational Dynamics Model to Explain the Ionic Strength Dependence of FMN –Heme Electron Transfer in Nitric Oxide Synthase

Andrei V. Astashkin,[1] Jinghui Li,[2] Huayu Zheng,[2,3] Yubin Miao,[4] Changjian Feng[2,3*]

[1] *Department of Chemistry and Biochemistry, University of Arizona, Tucson, AZ 85721, USA*
[2] *College of Pharmacy, University of New Mexico, Albuquerque, NM 87131, USA*
[3] *Department of Chemistry and Chemical Biology, University of New Mexico, Albuquerque, NM 87131, USA*
[4] *University of Colorado Denver, Radiology, Denver, CO 80045, USA*

[*] Corresponding author. E-mail address: cfeng@unm.edu

Table of Contents

1. Tethered shuttle model of NOS

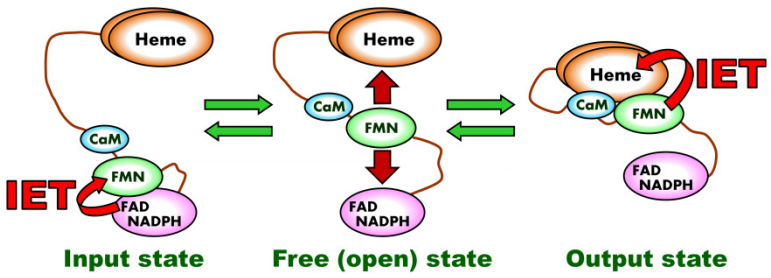

Figure S1. Tethered shuttle model. The FMN domain shuttles between its docking positions at the NADPH/FAD binding domain (where it acts as an electron acceptor) and heme domain (where it acts as an electron donor). The corresponding functional states of NOS are referred to as the (electron-accepting) input and (electron-donating) output states. Free FMN domain conformations also exist in between the two docked states.

2. CO rebinding rate constants determined by LFP

Table S1. CO rebinding rates in human iNOS oxyFMN (k_{CO}) and iNOSoxy (k_{AR}).

Ionic strength (mM)	k_{CO} (s^{-1})[a]	k_{AR} (s^{-1})[a]
100	1.34 ± 0.04	4.57 ± 0.10
150	1.64 ± 0.05	6.37 ± 0.11
200	1.04 ± 0.02	4.25 ± 0.09
250	1.49 ± 0.06	5.74 ± 0.11
300	1.18 ± 0.02	4.26 ± 0.06
400	1.12 ± 0.03	3.77 ± 0.07
500	1.67 ± 0.08	5.15 ± 0.10

[a] The cited errors are the average errors resulting from fitting of individual LFP traces.

The noise-like "dependence" of k_{CO} and k_{AR} on the ionic strength that can be seen in Table S1 is mostly the result of the variation in CO concentration between different sets of measurements. Because of the necessity to shut the gas valves at the input of the Ar/CO gas mixer for the night, the 3:1 Ar : CO gas mixture used for LFP measurements could only be prepared accurately for one set of measurements performed within one day, namely, for the measurement of k_{CO} and k_{AR} at the same ionic strength. For the next set of measurements on another day, the input valves were

reopened to reach the same flow rates, achieving the same Ar : CO ratio. However, since the achievable reproducibility of the flow rate could not be perfect, the resulting CO concentrations on different days of measurements were somewhat different. Therefore, although the CO rebinding rates determined at different ionic strengths are in the same ballpark, they show a random variation. The meaningful value obtained from these measurements is the ratio k_{CO}/k_{AR} determined under the same CO concentration, which allows one to estimate the ratio of intrinsic IET rates (see Eq. 2 and Table 1 in the main text).

One has to mention, though, that k_{CO} should actually depend on the ionic strength. Indeed, $k_{CO} = k_{AR}/(1+k_{ETf}/k_{ETb})$, as can be obtained from Eq. 2 of the main text. In this expression, k_{AR} = const (it is not expected to depend on the ionic strength, at least, as a first approximation, because CO is a neutral molecule), while k_{ETf}/k_{ETb} depends on the ionic strength (see Table 1 in the main text), and this dependence translates to k_{CO}. Practically, however, this dependence of k_{CO} is relatively weak (~20% over the studied range of ionic strength values), and is hidden under the noise-like variations caused by the differences in CO concentrations, as explained above.

3. FMN fluorescence lifetime data processing

A typical FMN fluorescence decay trace is shown by black trace in Fig. S2, and the instrument response function is shown by the red trace. For analysis in terms of amplitudes and dampings of the contributing exponential functions, the experimental fluorescence traces were deconvoluted from the instrument response function. This was achieved by:

i. Fourier transforming both traces into the frequency domain;
ii. Dividing the complex FT spectrum of the FMN trace by that of the instrument response function;
iii. Fourier transforming the quotient spectrum back into the time domain.

Because of strong phase noise in the quotient spectrum at high frequencies (resulting mostly from the noise in the denominator spectrum, which becomes relatively more important towards high frequencies because there the denominator amplitude decreases), the quotient spectrum was truncated at the frequency of 6 GHz. This resulted in a small-amplitude oscillation with 6 GHz frequency observed in the deconvoluted time domain fluorescence trace shown in Fig. 3 of the main text.

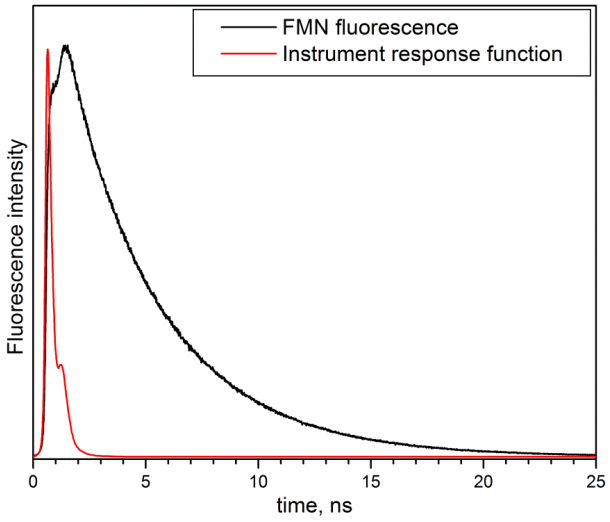

Figure S2. Black trace, FMN fluorescence trace recorded for the ionic strength of 100 mM. Red trace, instrument response function obtained for the same experimental setup.

4. Simplified structural model of iNOS oxyFMN construct (Fig. 5, main text)

Although the structural modules of NOS considered in this work (i.e., the heme and FMN domains and CaM) are not spherical, it is convenient to approximately represent them by spheres in order to be able to make analytical estimates of the docking energy (using Eq. 3 of the main text) and the rate constant for the docked state formation (Eq. 6 of the main text). The characteristic radii of these spheres were obtained by averaging the characteristic sizes of the corresponding NOS domains and bound CaM, using the structural information available in the protein databank (www.rcsb.org), *e.g.*, pdb 1NSI (for iNOS heme domain) and 3HR4 (human iNOS CaM and reductase domain complex).

The length of the tether between the heme and FMN domains is estimated as:

$$L = (3.8\ \text{Å}) \times n_{RC} + (1.5\ \text{Å}) \times n_{\alpha h}$$

where n_{RC} is the number of residue – residue intervals in the random coil sections of the tether and $n_{\alpha h}$ is the number of residue-residue intervals in the α-helical CaM-binding section. The random coil sections consist of residues 499 – 514 and 535 – 537, which results in n_{RC} = (515-498) + (538-534) = 21 (where 498 is the last α-helix residue of the heme domain and 538 is the 1st β-strand residue of the FMN domain). The α-helical part of the tether consists of residues 515 – 534, which results in $n_{\alpha h}$ = 19. The tether length is thus estimated as L = 108.3 Å. In the manuscript, this value was rounded to 110 Å.

For comparison, in an extended conformation of rat nNOS, the edge-to edge distance between the FMN and heme domains can be estimated as ~ 80 Å from the single molecule cryo-EM images in ref. 9 of the main text. This distance obviously represents the lower bound of the tether length. Most likely, it is close to the most probable end-to-end distance for the tether, and thus it should be significantly shorter than the actual length. Unfortunately, since the detailed conformational statistics for the FMN-heme domain tether is not known (a calculation of such a statistics, including the volume exclusion effects, represents a complex mathematical problem), it is not possible to accurately estimate the length of fully extended tether from the distance of 80 Å.

Therefore, we can only state the qualitative agreement between our estimate of the full tether length (~110 Å) with the cryo-EM observations.

5. Note on estimating the volumes and orientation ranges available for the tethered FMN domain in the undocked and docked states (i.e., V, Ω, and ψ parameters in Eq. 3, main text)

1). To estimate the volume V_u accessible for the tethered FMN domain in the undocked state, one has to take into account the limitations on the FMN domain position imposed by the sizes of the FMN and heme domains and the tether length. These limitations can be understood from Fig. S3. This Figure shows the vertical crossection of several 3D regions (I, II, and III), which have cylindrical symmetry with respect to axis Z. Regions I and II are accessible for the FMN domain center, while region III is not. The latter region represents a sphere with the radius $R = R_{heme} + R_{FMN} \sim 50$ Å.

Region I is a hemisphere of radius $L \sim 110$ Å (L is the tether length), and its volume is readily calculated as $V_I = \frac{2}{3}\pi L^3 = 2.79 \cdot 10^6$ Å^3.

Region II is more complicated because its shape is defined by partial or complete wrapping of the FMN – heme domain tether around the heme domain. This region resembles a doughnut bounded on the outside by the surface, whose points are located at the distance $L_1 = L + 2R(\sin\alpha - \alpha)$ from the tether origin, where α is the angle between the $\mathbf{L_1}$ radius vector and the horizontal (XY) plane passing through the tether origin (see Fig. S3 for all parameters). The inner boundary of region II represents the surface of the sphere confining region III. The easiest way to calculate the volume of region II is numerical integration. This results in $V_{II} = 2.10 \cdot 10^6$ Å^3, and the total available volume is thus $V_u = V_I + V_{II} \approx 4.89 \cdot 10^6$ Å^3, which is rounded in the main text to $5 \cdot 10^6$ Å^3.

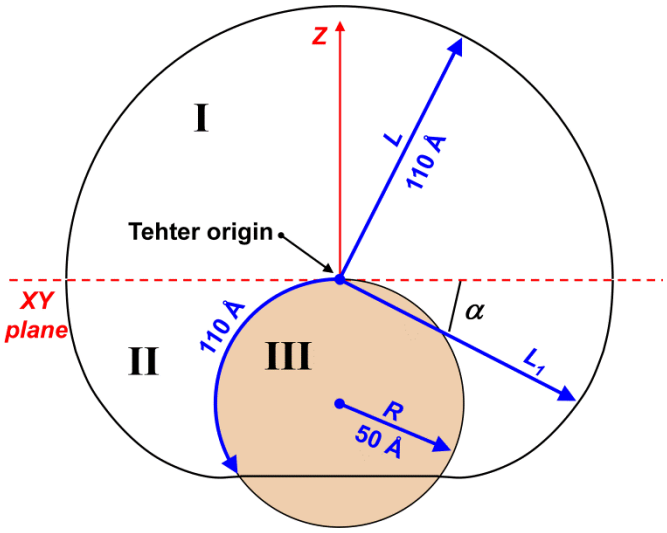

Figure S3. Explanation of parameters used to calculate the volume available to the undocked FMN domain tethered to the heme domain in NOS. The actual 3D representation can be obtained by rotation around the symmetry axis Z. Regions I and II are outside the heme domain and are allowed

for the undocked FMN domain, while region III is inside the heme domain and is not allowed. The parameters are as follows: $L \sim 110$ Å is the FMN – heme domain tether length; $R \sim 50$ Å is the radius of the "excluded" region III equal to the sum of the radii of the FMN and heme domains. $L_1 = L + 2R(\sin\alpha - \alpha)$ is the maximum extension of the tether in the lower hemisphere (below the XY plane) with taking into account the tether wrapping around the heme domain. The angle α is between the $\mathbf{L_1}$ radius vector and the XY plane.

The rest of parameters describing the available volume and orientation ranges entering Eq. 3 of the main text are more straightforward:

2). $V_d = \pi R_D d_{max} \sim 10^3$ Å^3, where $R_D \sim 7 - 8$ Å is the radius of the docking area and $d_{max} \sim 5$ Å is the maximum possible distance between the FMN and heme domain surfaces in the docked state.

3). $\Omega_u \sim 4\pi$ is the range of angular orientations of the FMN domain in the undocked state. It simply equals to the solid angle corresponding to the complete sphere.

4). $\Omega_d \sim 2\pi\cdot(1-\cos\theta/2) \sim 1$ is the range of angular orientations of the FMN domain in the docked state. It is estimated as the solid angle corresponding to the docking area as seen from the center of the FMN domain. In the above expression, $\theta \sim 1$ is the angular size of the docking area (~ 15 Å in diameter) as seen from the center of the FMN domain (which has a radius of ~ 15 Å).

5). $\psi_u = 2\pi$ is the range of orientations of the FMN domain with respect to the normal passing through the center of the docking area when the FMN domain is undocked. In the undocked state, all orientations are possible, and thus $\psi_u = 2\pi$.

6). $\psi_d \sim 2R_D/(R_{FMN}+R_{CaM}) \sim 0.5$ is the range of orientations of the FMN domain with respect to the normal passing through the center of the docking area when the FMN domain is docked to the heme domain. In the docked state, this rotation freedom is limited by CaM, which docks to the heme next to the FMN domain. Both CaM and FMN domains should have their docking areas overlapped with those of the heme domain, which obviously results in the above expression for ψ_d. In this expression, $2R_D \sim 15$ Å is the characteristic diameter of the docking area, and R_{FMN} and R_{CaM} (both equal to ~ 15 Å) are the characteristic radii of the FMN domain and CaM, respectively.

6. Stationary solution of the kinetic equation (Eq. 17, main text)

In the stationary limit (i.e., $[\dot{A}] = 0$), the kinetic equation given by Eq. 17 of the main text becomes:

$$-[A]([A]+[B]_o-[A]_o)+k_d([A]_o-[A])=0 \qquad \text{(S1)}$$

where $k_d = k_{off}/k_{on}$ and the balance equations (2nd and 3rd lines in Eq. 17) have been used. The exact solution of Eq. S1 with respect to [A] is:

$$[\mathrm{A}] = \frac{-k_\mathrm{d} + [\mathrm{A}]_\mathrm{o} - [\mathrm{B}]_\mathrm{o} + \sqrt{(k_d - [\mathrm{A}]_\mathrm{o} + [\mathrm{B}]_\mathrm{o})^2 + 4k_d[\mathrm{A}]_\mathrm{o}}}{2} = \frac{-k_\mathrm{d} + [\mathrm{A}]_\mathrm{o} - [\mathrm{B}]_\mathrm{o} + \sqrt{(k_\mathrm{d} + [\mathrm{A}]_\mathrm{o} + [\mathrm{B}]_\mathrm{o})^2 - 4[\mathrm{A}]_\mathrm{o}[\mathrm{B}]_\mathrm{o}}}{2} \tag{S2}$$

where only the positive square root is meaningful. Expanding the root to the linear term results in:

$$[\mathrm{A}] \approx [\mathrm{A}]_\mathrm{o} - \frac{[\mathrm{A}]_\mathrm{o}[\mathrm{B}]_\mathrm{o}}{k_\mathrm{d} + [\mathrm{A}]_\mathrm{o} + [\mathrm{B}]_\mathrm{o}} = \frac{(k_\mathrm{d} + [\mathrm{A}]_\mathrm{o})[\mathrm{A}]_\mathrm{o}}{k_\mathrm{d} + [\mathrm{A}]_\mathrm{o} + [\mathrm{B}]_\mathrm{o}} = \frac{[\mathrm{A}]_\mathrm{o}}{1 + [\mathrm{B}]_\mathrm{o}/(k_\mathrm{d} + [\mathrm{A}]_\mathrm{o})} \tag{S3}$$

which reproduces Eq. 18 of the main text.